

High-Throughput Kinetic Study of Hydrogenation over Palladium Nanoparticles: Combination of Reaction and Analysis

Oliver Trapp,* Sven K. Weber, Sabrina Bauch, Tobias Bäcker, Werner Hofstadt, and Bernd Spliethoff^[a]

Abstract: The hydrogenation of 1-acetylcyclohexene, cyclohex-2-enone, nitrobenzene, and *trans*-methylpent-3-enoate catalyzed by highly active palladium nanoparticles was studied by high-throughput on-column reaction gas chromatography. In these experiments, catalysis and separation of educts and products is integrated by the use of a catalytically active gas chromatographic stationary phase, which allows reaction rate measurements to be efficiently performed by employing reactant libraries. Palladium nanoparticles embedded in a stabilizing polysiloxane matrix serve as catalyst and selective chromatographic stationary phase for these multiphase reac-

tions (gas–liquid–solid) and are coated in fused-silica capillaries (inner diameter 250 μm) as a thin film of thickness 250 nm. The palladium nanoparticles were prepared by reduction of palladium acetate with hydridomethylsiloxane–dimethylsiloxane copolymer and self-catalyzed hydrosilylation with methylvinylsiloxane–dimethylsiloxane copolymer to obtain a stabilizing matrix. Diphenylsiloxane–dimethylsiloxane copolymer (GE SE 52) was added to improve film stability over a

wide range of compositions. Herein, we show by systematic TEM investigations that the size and morphology (crystalline or amorphous) of the nanoparticles strongly depends on the ratio of the stabilizing polysiloxanes, the conditions to immobilize the stationary phase on the surface of the fused-silica capillary, and the loading of the palladium precursor. Furthermore, hydrogenations were performed with these catalytically active stationary phases between 60 and 100 °C at various contact times to determine the temperature-dependent reaction rate constants and to obtain activation parameters and diffusion coefficients.

Keywords: gas chromatography • hydrogenation • kinetics • nanoparticles • palladium

Introduction

The discovery of highly productive and selective catalysts and the expansion of synthetic techniques and methods in chemistry is of substantial interest for both science and industry. For the directed design of catalysts, comprehensive kinetic and thermodynamic data of existing catalytic systems are necessary to understand how the catalytic mechanism might be controlled by structural parameters.^[1,2] This requires the measurement of large sets of kinetic data for a broad variety of substrates. From these data, models can be developed and refined to identify rate-controlling elementary steps to gain insight into the reaction mechanism on a

molecular level. Nowadays, various high-throughput screening techniques are available, for example, (time-resolved) IR thermography,^[3] resonance-enhanced multiphoton ionization (REMPI),^[4] scanning mass spectrometry,^[5] visual detection with reactive dyes,^[6] UV/Vis spectroscopy,^[7] fluorescence-based assays,^[8] nondispersive IR (NDIR) analysis,^[9] circular dichroism (CD) for screening of enantioselective catalysts, and acoustic-wave sensor systems,^[10] which allow the investigation of comprehensive catalyst libraries. Chromatographic techniques^[11] have the advantage that even complex reaction mixtures can be separated and quantified without any tagging with marker molecules to make analytes detectable by a specific detector. Consistent enhancements in the field of parallelized kinetic measurements of catalysts with minute material consumption^[12] are achieved with microfluidic devices, which combine chemical synthesis and analysis on the same chip.^[13] However, a major drawback of commonly used batch reactors is the limitation of studying only one reaction per run. The reaction, separation, and quantification of the educts and products to determine

[a] Dr. O. Trapp, S. K. Weber, S. Bauch, T. Bäcker, W. Hofstadt, B. Spliethoff
Max-Planck-Institut für Kohlenforschung
Kaiser-Wilhelm-Platz 1, 45470 Mülheim an der Ruhr (Germany)
Fax: (+49)208-306-2995
E-mail: trapp@mpi-muelheim.mpg.de

conversions have to be performed consecutively because competing reactions lead to indefinable reaction kinetics. Recently, we reported a strategy that allows the synchronous combination of catalysis and separation in capillaries to perform high-throughput reaction rate measurements (on average 147 reactions h⁻¹) of reactant libraries for hydrogenation over highly active palladium nanoparticles.^[14]

We focused on hydrogenation reactions as this chemical transformation is one of the most important and widely used catalytic reactions in synthetic chemistry.^[15] Hydrogenations can be catalyzed by stabilized Pd and Pt nanoparticles,^[16] which have become the focus of increasing interest in catalysis in recent years due to their high activity under mild reaction conditions.^[17] However, multiphase catalytic systems (gas–liquid–solid), which are typically used in industrial applications, are difficult to investigate as the interaction of the reactant with the catalyst is controlled by the mass transfer between the different phases, and therefore the apparent reaction rate is composed of the inherent reaction rate and diffusion rates. To reduce this effect, the interfacial area has to be increased. Microstructured reaction systems intrinsically have a high specific interfacial area per volume ($a_{\text{inter}} = 2/r$), which is only dependent on the radius of circular reaction channels, that is, for microcapillaries with inner diameters (i.d.) between 250 and 100 μm the specific interfacial area per volume ranges from 16000 to 40000 m²m⁻³.

Furthermore, nanoparticles show extraordinary catalytic activity because of high surface-to-volume ratios. The particle size and the morphology of Pd nanoparticles, as well as the nature of the stabilizing matrix to prevent agglomeration, correlate with their catalytic activity.

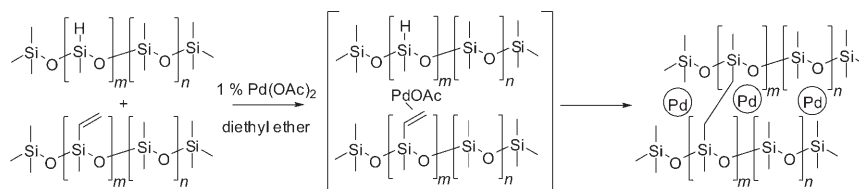
There are numerous examples describing hydrogenations^[17] and C-C coupling reactions^[18] catalyzed by Pd nanoparticles or formation of Pd nanoparticles from Pd complexes in the course of the reaction. Despite the large number of publications, further insights into the dependency of these quasi-homogeneous reactions on the size and morphology of the nanoparticles are necessary to understand how their structure controls the reaction mechanism.^[19]

Herein, we show by systematic TEM investigations that the size and morphology (crystalline or amorphous) of the nanoparticles strongly depends on the ratio of the stabilizing polysiloxanes, the activation temperature to immobilize the stationary phase on the surface of the capillary, and the loading of the Pd precursor. Hydrogenations were performed with these catalytically active stationary phases between 60 and 100 °C at various contact times by on-column reaction gas chromatography to determine temperature-dependent reaction rate constants and to obtain activation parameters (ΔG^\ddagger , ΔH^\ddagger , ΔS^\ddagger) with a kinetic model based on

the Langmuir–Hinshelwood mechanism. From these experiments, the diffusion coefficients of the substrates in the polysiloxane matrix were also obtained.

Results and Discussion

Preparation of Pd nanoparticles embedded in a polysiloxane matrix: To control the growth of Pd nanoparticles and to prevent them from agglomeration, surfactants are typically used, for example, quaternary ammonium salts, which form a monolayer on the surface of the nanoparticles and stabilize them by steric and electrostatic effects.^[16d] The protecting shell also controls the interaction of the substrate with the active site on the nanoparticles and consequently the catalytic activity. Taking this into consideration and making the protecting shell compatible with a chromatographic stationary phase, so that the catalytic system can be investigated by on-column reaction gas chromatography, the following strategy was developed. Pd nanoparticles were embedded in a polysiloxane matrix by using vinylpolysiloxane and hydridopolysiloxane, which acts as reducing agent^[20] and cross-linked by hydrosilylation at the same time. Therefore, we prepared a methylvinylsiloxane–dimethylsiloxane copolymer (MVPS, 4.5% Si(O)(CH₃)(CH=CH₂) groups) to coordinate Pd(OAc)₂ to the vinyl groups in diethyl ether. To reduce Pd²⁺ to Pd⁰ and to obtain an inert protecting matrix for the Pd nanoparticles, a hydridomethylsiloxane–dimethylsiloxane copolymer^[21] (HMPS, 25.7% Si(O)(CH₃)H groups) was added to this mixture. Cross-linking with the MVPS was achieved by hydrosilylation, catalyzed in the presence of Pd(OAc)₂ and the Pd nanoparticles (Scheme 1). By ¹H NMR



Scheme 1. Preparation of highly active Pd nanoparticles embedded in a polysiloxane matrix.

spectroscopic measurements, we could confirm that the percentage of Si(O)(CH₃)H groups starting from 16.1%, exemplified for a mixture of Pd(OAc)₂ (0.1 mg), HMPS (10 mg, 25.7% Si(O)(CH₃)H groups), and MVPS (6 mg, 4.5% Si(O)(CH₃)(CH=CH₂) groups), decreased to 2.6%.

We observed by TEM measurements that the size and morphology of the Pd nanoparticles depends on the ratio of the stabilizing polymers, the activation conditions (under a hydrogen atmosphere, temperature), and the concentration of the Pd precursor. The obtained Pd nanoparticles stabilized by a 3:1 ratio of the two polysiloxanes (HMPS/MVPS) are spherical and crystalline with a narrow size distribution of (3.2 ± 0.7) nm^[14] determined by TEM (Figure 1a). After treatment with hydrogen at an elevated temperature

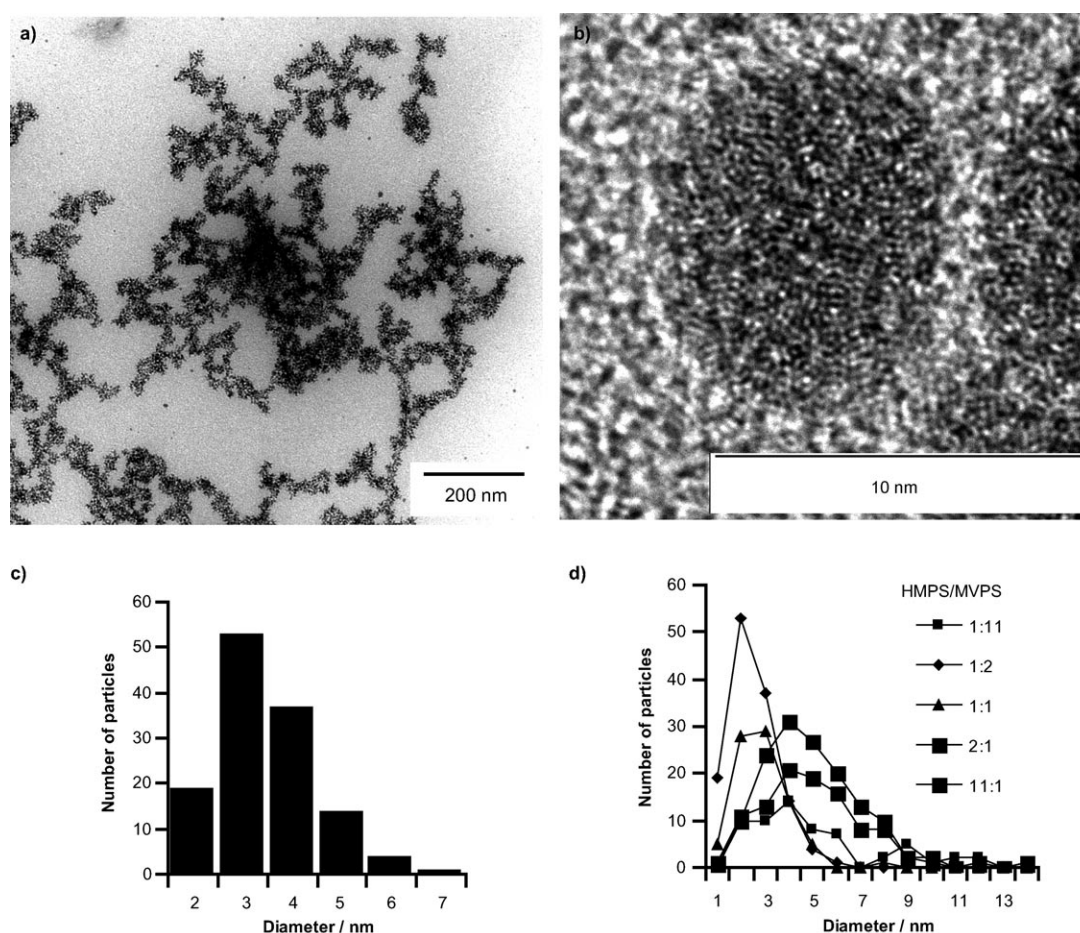


Figure 1. a) Overview TEM image of Pd nanoparticles showing the homogeneous size distribution; b) TEM image of amorphous nanoparticles; c) size distribution of Pd nanoparticles with a ratio of HMPS/MVPS 1:2 and mean diameter (3.0 ± 1.0) nm; and d) size distribution of Pd nanoparticles depending on the ratio of the stabilizing polysiloxanes before heat treatment under a hydrogen atmosphere.

(200°C), we also found amorphous nanoparticles^[22] (Figure 1b) with an increased size of (3.6 ± 1.6) nm, which can be attributed to the formation of Pd hydride and also agglomeration processes at these elevated temperatures. Surprisingly, the size is also controlled by the ratio of the two polysiloxanes. To study this effect systematically, we prepared 40 Pd nanoparticle samples by variation of both the mixture of the two polysiloxanes and the Pd loadings (Table 1). It is important to note that for these experiments we added the slightly polar stationary phase GE SE 52 to the polysiloxane mixture to improve the stability of coatings on the inner surface of fused-silica capillaries. The addition of the GE SE 52 has the effect of making the particle sizes larger because of the dilution effect of the two cross-linking polysiloxanes.

Table 1. Particle sizes and distributions and their dependency on the polysiloxane ratio before and after heat treatment under a hydrogen atmosphere.^[a] The conversions C , rate constants k , and Gibbs activation energies ΔG^\ddagger are given for the hydrogenation of cyclohex-2-enone.

Ratio HMPS/MPVS	Particle size after preparation [nm]	Particle size $200^\circ\text{C}/\text{H}_2$ [nm]	C [%]	k [s^{-1}]	ΔG^\ddagger [kJ mol^{-1}]
1:11	5.5 ± 2.8	11.0 ± 6.2	66.4	2.27	79.6
1:2	3.0 ± 1.0	3.6 ± 1.6	88.2	4.85	77.5
1:1	3.4 ± 1.1	3.4 ± 1.5	49.4	1.56	80.7
2:1	5.4 ± 2.0	5.5 ± 1.8	37.1	1.07	81.7
11:1	5.4 ± 2.0	5.9 ± 2.5	82.5	3.87	78.2

[a] Samples were prepared from the mixture of HMPS and MPVS (24 mg), GE SE 52 (24 mg), and $\text{Pd}(\text{OAc})_2$ (0.3 mg). The Pd concentration was $1.1 \times 10^{-10} \text{ mol cm}^{-1}$ fused-silica capillary for the catalytic testing at 60°C and 100 kPa H_2 , by using a 3 cm capillary.

As described above, the MVPS coordinates the $\text{Pd}(\text{OAc})_2$ through vinyl groups while the HMPS is needed for the reduction of Pd^{2+} to Pd^0 and the cross-linking of the polymer matrix. Taking into account that the content of $\text{Si}(\text{O})(\text{CH}_3)(\text{CH}=\text{CH}_2)$ groups in the MVPS is 4.5% and the content of $\text{Si}(\text{O})(\text{CH}_3)\text{H}$ groups in the HMPS is 25.7%, a 1:6 ratio of the two polymers (HMPS/MVPS) should lead to complete cross-linking. However, HMPS is also needed to reduce

Pd^{2+} to Pd^0 , and therefore to achieve completion of the reaction an HMPS/MVPS ratio ranging from at least 1:1 to 3:1 is required. The size distribution of the nanoparticles measured by TEM for five selected ratios of the two stabilizing polysiloxanes (HMPS/MVPS 1:11, 1:2, 1:1, 2:1, 11:1) indicates that a 1:2 mixture leads to smaller Pd nanoparticles with a narrow size distribution (Figure 1c and Table 1).

Pd nanoparticles prepared with a polysiloxane ratio of HMPS/MVPS 1:11 show an increased particle size and a broader size distribution. To study the effect of hydrogen on the size and morphology of the Pd nanoparticles, Cu grids for TEM analysis were coated with the viscous brownish-gray polysiloxanes and then treated with hydrogen at 200 °C. It was found that high HMPS and low MVPS concentrations, lead to pronounced agglomeration of the particles with a broad size distribution (11.0 ± 6.2 nm; see Table 1).

The dependency of nanoparticle formation on the particle size and distribution of the two polysiloxanes can be explained by kinetic effects. The reduction of Pd^{2+} to Pd^0 is compared to the hydrosilylation leading to cross-linking and stabilization of the nanoparticles in a fast process. It can be assumed that in a first step, seeds of small Pd nanoparticles are formed which agglomerate to form the resulting nanoparticles. This process is controlled by diffusion. The MVPS used here is less viscous than HMPS, which should allow easier diffusion of the nanoparticles resulting in the observed agglomeration to larger particles. Samples prepared with a high HMPS concentration form Pd nanoparticles quickly, which can be observed by a darkening of the solution. The agglomeration itself is controlled by diffusion and by the rate of the cross-linking of the two polysiloxanes, which dynamically increases the viscosity and decreases diffusion of the particles.

Catalytic studies by on-column

reaction chromatography: To perform kinetic investigations of hydrogenation over the prepared Pd nanoparticles, solutions of the polysiloxanes with the embedded Pd nanoparticles were used to coat fused-silica capillaries (i.d. 250 μm , film thickness 250 nm) by the static method described by Grob.^[23] For the activation of the Pd nanoparticles and to permanently bond the polysiloxanes to the fused-silica capillary by reaction of surface silanol groups with the remaining hydrosilylation groups, the fused-silica capillaries were heated to 200 °C at a rate of 0.5 K min^{-1} under slow hydrogen flow. It was found that polymers prepared with an excess of HMPS gave more stable films not leading to drop-

let formation, which indicates destruction of the polymer film. However, to compare the catalytic properties of the Pd nanoparticles with the varying polysiloxane compositions, the slightly polar stationary phase GE SE 52 (polysiloxane containing 5% phenyl groups) was added to the mixture. On-column catalysis experiments were performed by coupling the Pd nanoparticle microcapillaries (length = 2.02, 2.90, 3.84, 5.10, 6.15 cm) between a pre-separation capillary (1 m) and a separation column (25 m), which were installed in a gas chromatograph. The purpose of the pre-separation column was to thermally equilibrate the reactants and to spatially separate the educts of the injected compound library, which enabled high-throughput kinetic investigations due to the absence of competing reactions. Hydrogen was used as a reactive carrier gas. Reaction educts and products were detected by flame ionization detection (FID) for quantification and identified by quadrupole ion-trap mass spectrometry. The educt library consisting of four unsaturated and functionalized compounds (1-acetylcyclohexene, cyclohex-2-enone, nitrobenzene, and *trans*-methylpent-3-enoate) was simultaneously injected onto this column configuration at different temperatures (60–100 °C) and inlet pressures (60–100 kPa) to vary the reaction time and to obtain temperature-dependent kinetic data (Figure 2).

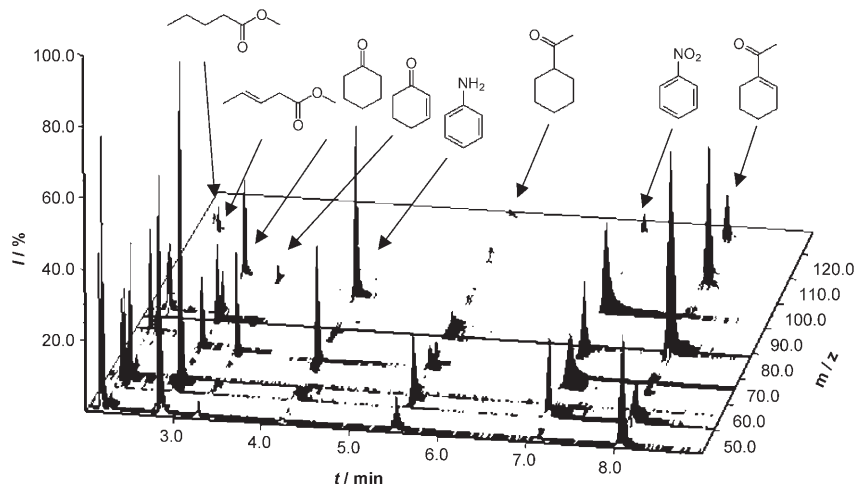


Figure 2. Expanded image (2–9 min) of the gas chromatographic separation and mass traces of the on-column hydrogenation of the four substrates at 70 °C and 100 kPa.

By the use of educt libraries and measurement of reaction rate constants of the spatially separated compounds, an extraordinarily high throughput can be realized. Recently, we demonstrated that for a library consisting of 22 compounds a throughput of 5880 reactions in 40 h could be achieved. Here, we screened systematically varied sets of fused-silica capillaries coated with Pd nanoparticles embedded in a polysiloxane matrix, by changing the ratio of stabilizing polysiloxanes (see Table 1) and the Pd loading, under different reaction conditions (temperature, contact time) and with variation of the column length.

The conversions and rate constants for the hydrogenation of cyclohex-2-ene varied in a broad range for the individual polysiloxane ratios (see Table 1). These data (in total 370 experiments were performed) can be interpreted by taking the particle sizes and the degree of cross-linking of the polysiloxanes into consideration. Higher conversions are observed for small particles than for larger particles. However, the reaction rate constant is also influenced by the degree of cross-linking, which controls the accessibility of the nanoparticles by the substrates. For nanoparticles only stabilized by the viscosity of the linear polysiloxane chains, higher conversions, even for larger nanoparticles, are observed (1:11 and 11:1 for HMPS/MVPS). To make a compromise between particle size, stabilization, and activity, a polysiloxane ratio of 3:1 for HMPS/MVPS was chosen for further experiments, because under these conditions the Pd nanoparticles do not agglomerate when heated.

The dependency of the conversion on the column length is the prerequisite for on-column reaction chromatography to determine kinetic data.^[24] The contact time should correlate with the length of the capillary and the catalytic activity must not change. It is important to note that this correlation is only given for diluted samples, because overloading of the stationary phase leads commonly to nonlinear effects.^[25]

To prove that the contact time correlates with the length of the capillary, the hydrogenation reactions of the substrates were performed at 80 °C by using different capillary lengths (2.02, 2.90, 3.84, 5.10, 6.15 cm) at a constant Pd loading of $7.28 \times 10^{-11} \text{ mol cm}^{-1}$ (see Table 2; medium concentra-

Table 2. Variation of the Pd concentration (50% GE SE 52, HMPS/MVPS 3:1).

Capillary length [cm]	Pd [mg]	Pd loading [$10^{-11} \text{ mol cm}^{-1}$]
5.10	0.05	3.64
2.90	0.10	7.28
2.02	0.20	14.56

tion of the three Pd concentrations investigated, HMPS/MVPS 3:1), which resulted in different reaction times in the range of 76 to 1690 ms (Figure 3). For longer capillaries (> 6 cm) or higher Pd concentrations, we observed complete conversion for some of the substrates, for example, 99.9% conversion for *trans*-methylpent-3-enoate on a 6.15 cm capillary.

Additionally, we systematically varied the Pd nanoparticle loading in the fused-silica capillaries (see Table 2) and performed catalytic tests with the four hydrogenation educts. We found that in this concentration range, the conversion of the educts and hence the catalytic activity of the Pd nanoparticles linearly correlates with the Pd concentration of the Pd precursor. We can conclude that the hydrogenation proceeds according to a first-order reaction with regard to Pd. Figure 4 shows the conversion as a function of the Pd loading on the capillary for the different substrates. However, it has to be pointed out that for increasing Pd concentrations,

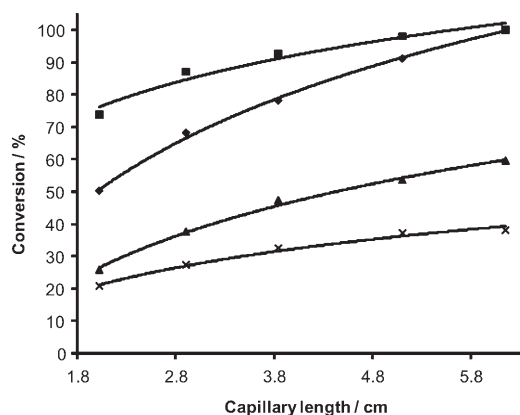


Figure 3. Educt conversion at 80 °C and 80 kPa versus the column length for *trans*-methylpent-3-enoate (◆), cyclohex-2-ene (■), nitrobenzene (▲), and 1-acetylcyclohexene (×).

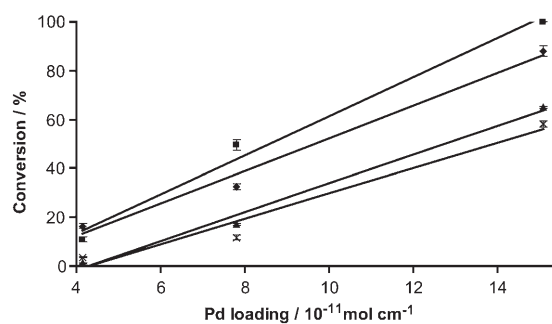


Figure 4. Educt conversion versus the Pd loading for *trans*-methylpent-3-enoate (◆), cyclohex-2-ene (■), nitrobenzene (▲), and 1-acetylcyclohexene (×).

which lead to larger particles because of agglomeration, the relative surface area is decreased compared to small nanoparticles and therefore a nonlinear decrease of the catalytic activity is expected.

To investigate this dependency in greater detail, we performed temperature- and flow-dependent conversion measurements to obtain three-dimensional datasets (temperature, reaction time, conversion) for each compound. All measurements were repeated three times at 60, 70, 80, 90, and 100 °C and hydrogen inlet pressures of 60, 70, 80, 90, and 100 kPa. Note that the resulting conversion surface functions are not flat planes, which can be attributed to the fact that the residence time strongly depends on the separation efficiency of the reactor column. The separation efficiency is a function of the temperature and the flow rate and is described by the van Deemter equation (see below). The evaluation of these datasets gives the activation parameters, which can be correlated with the Pd loading of the capillaries and also the composition of the polysiloxanes (Figure 5).

Determination of reaction rate constants and activation parameters: The hydrogenation of unsaturated compounds

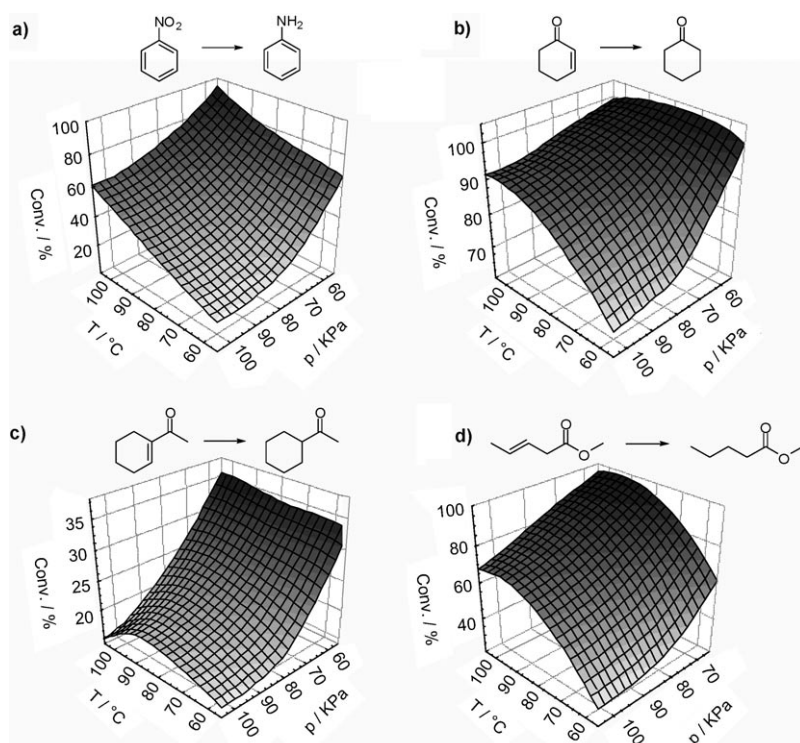
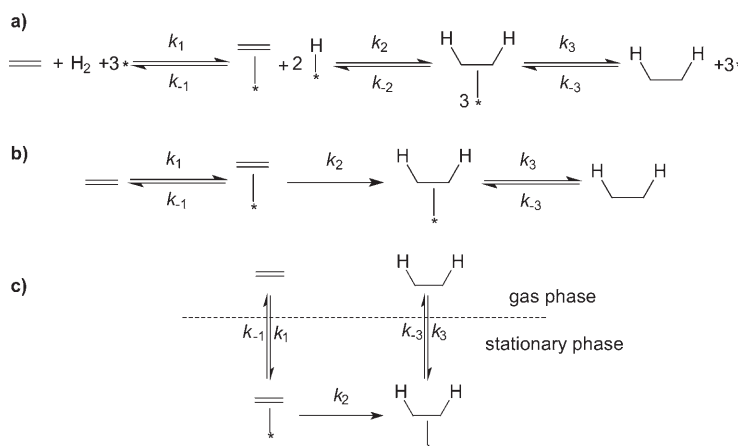


Figure 5. 3D plots of the conversion of the hydrogenations of nitrobenzene (a), cyclohex-2-enone (b), 1-acetylcyclohexene (c), and *trans*-methylpent-3-enoate (d) at different temperatures (60–100 °C) and inlet pressures (60–100 kPa).

over Pd surfaces is typically described by a Langmuir–Hinshelwood mechanism.^[26] To use this model for the evaluation of the experimental data, the following concept has been elaborated to adapt it to the on-column reaction chromatographic experiment. The Langmuir–Hinshelwood mechanism is depicted in Scheme 2a, in which the substrates are represented as a double bond and the catalytically active sites by an asterisk in the following mechanistic description, considering, in particular, the diffusion-limited steps (adsorption and desorption of educts and products).



Scheme 2. Hydrogenation of the substrates described by a Langmuir–Hinshelwood mechanism. Substrates are represented as a double bond (=) and the catalytically active sites by an asterisk (*).

Considering our experimental conditions in on-column reaction chromatography, the following assumptions can be made. 1) H₂ is used as a reactive carrier gas at a high flow rate in the range of mL min⁻¹, and thus there is an excess of H₂ compared to the substrates (typically H₂/substrate 99.99999:0.00001). 2) The adsorption of H₂ on the Pd surface is fast because the activation energy for this process is very low and H₂ easily passes the polysiloxane matrix. This means that there is a steady state of hydrogen adsorbed on the Pd nanoparticles, which does not influence the intrinsic hydrogenation rate of the substrate. 3) Compared to the substrate there is an excess of Pd nanoparticles, so that there are enough reactive sites available for the adsorption of the reaction educt. 4) The hydrogenation of the substrates can be considered as an irreversible

process to the hydrogenated product. Dehydrogenation in the presence of Pd is only expected at higher temperatures, typically higher than at least 150 °C, because here the limiting step is the desorption of hydrogen from the metal.^[27] Consideration of these points simplifies the model in the on-column reaction chromatographic setup to the key steps depicted in Scheme 2b. The advantage of this chromatographic experiment is that the transport by diffusion of the substrate to the catalytically active site can be considered orthogonal to the hydrogenation process itself. The distribution equilibria of the educts and products are obtained by the retention parameters, and diffusion coefficients can be determined by temperature- and flow-dependent measurements of the separation efficiency by using the retention times and peak width of the individual substrates. Therefore, the model depicted in Scheme 2b can be applied to every chromatographic theoretical plate, which can be considered as a catalytic chromatographic reactor (Scheme 2c). This means that with the known retention parameters given the residence time of the substrate, the reaction time is defined and reaction rate constants can be calculated from the conversion data by using a first-order reaction rate law according to Equation (1):

$$-\frac{d(\text{substrate})}{dt} = k_2[\text{substrate}] \quad (1)$$

This expression is independent of the absolute concentra-

tions of the substrates. Notably, the conversions were determined from the data for gas chromatography with FID, which gives signal intensities that can be correlated to the ionizable carbon atoms in a specific molecule. This means that the signal intensities of the hydrogenated product and educt are the same and therefore no correction factor has to be applied.

Residence times of the hydrogenation educts were determined with a reference column by using the same composition of the stationary phase as for the catalytically active capillary columns. Reaction rate constants, k , of hydrogenation were determined by application of Equation (1) to the conversion data. The Gibbs free activation energies $\Delta G^\ddagger(T)$ were calculated according to the Eyring equation [Eq. (2)] with k_B as the Boltzmann constant ($k_B = 1.380662 \times 10^{-23} \text{ J K}^{-1}$), T as the reaction temperature (K), h as Planck's constant ($h = 6.62617 \times 10^{-34} \text{ J s}$), and R as the gas constant ($R = 8.31441 \text{ J K}^{-1} \text{ mol}^{-1}$). The statistical factor κ was set to 1.0.

$$\Delta G^\ddagger(T) = -RT \ln \left(\frac{k_1 h}{\kappa k_B T} \right) \quad (2)$$

Activation parameters were calculated from temperature-dependent measurements. The activation enthalpy ΔH^\ddagger of the reaction was obtained from the slope and the activation entropy ΔS^\ddagger from the intercept of the Eyring plot ($\ln(k_1/T)$ as a function of T^{-1}). Deviations of the activation parameters ΔH^\ddagger and ΔS^\ddagger were calculated by error-band analysis of the linear regression with a level of confidence of 95%.

Table 3 summarizes the conversions, reaction rate constants k , and activation parameters (ΔG^\ddagger , ΔH^\ddagger , ΔS^\ddagger) of the hydrogenation reactions of the four substrates for different Pd loadings. By applying pseudo-first-order reaction kinetics, a very good agreement with respect to the substrates

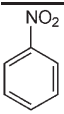
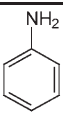
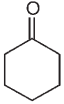
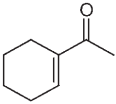
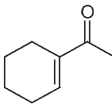
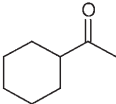
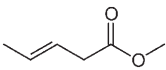
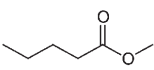
was achieved according to the Langmuir–Hinshelwood mechanism.

The high activity of the Pd nanoparticles is corroborated by the activation parameters, which show low activation enthalpies ΔH^\ddagger and negative activation entropies ΔS^\ddagger that correspond to a restrained transition state. Comparison of the activation parameters between 1-acetylcyclohexene, cyclohex-2-enone, and *trans*-methylpent-3-enoate shows that the less-hindered alkene (*trans*-methylpent-3-enoate) has the lowest activation enthalpies ΔH^\ddagger and activation entropies ΔS^\ddagger compared to the more hindered alkenes, for example, 1-acetylcyclohexene. For cyclohex-2-enone, the reaction rates are mainly dominated by the activation entropy ΔS^\ddagger , which results in high productivities.

As already pointed out, the reaction rate constants k increase with higher Pd loadings, which can be attributed to a linear dependency on the rate law of the active sites of the catalysts. This can be correlated to the Pd concentration under the described diluted conditions. We also found that the reaction rate constants were lower for the stabilizing matrix with GE SE 52 as the additive compared to the Pd nanoparticles, which are only stabilized by HMPS and MVPS.^[14] This finding suggests that the phenyl groups of the stationary phase GE SE 52 have an inhibiting effect on the hydrogenation reaction, probably caused by stabilization of the nanoparticles. Such stabilization effects for Pd nanoparticles have been also observed and used by Kobayashi et al.^[17a]

Determination of diffusion constants: In microfluidic systems, the control of mixing is often challenging, because diffusion rates contribute to the apparent reaction rates. In the present setup, diffusion processes can be quantified and experimentally controlled by the polysiloxane used. The van Deemter equation^[28] [Eq. (3)] was employed to determine diffusion coefficients:

Table 3. Selected results of the on-column hydrogenations over highly active Pd nanoparticles for three different palladium loadings.

Substrate	Product	Pd loading [$10^{-11} \text{ mol cm}^{-1}$]	$C^{[a]}$ [%]	$k^{[b]}$ [s^{-1}]	$\Delta G^{\ddagger [c]}$ [kJ mol^{-1}]	ΔH^\ddagger [kJ mol^{-1}]	ΔS^\ddagger [$\text{J K}^{-1} \text{ mol}^{-1}$]	$r^{[d]}$ (s.d.)
		3.64	1.2	0.03	91.3	68.3 ± 0.6	-77 ± 1	0.999 (0.028)
		7.29	17.2	0.29	84.1	69.4 ± 0.3	-49 ± 1	0.999 (0.034)
		14.6	65.0	1.05	82.1	76.5 ± 2.8	-19 ± 1	0.993 (0.102)
		3.64	10.8	0.94	79.9	39.3 ± 0.9	-136 ± 5	0.997 (0.045)
		7.29	49.7	3.83	75.8	53.5 ± 0.7	-75 ± 1	0.995 (0.073)
		14.6	100.0	$\text{—}^{[e]}$	$\text{—}^{[e]}$	$\text{—}^{[e]}$	$\text{—}^{[e]}$	$\text{—}^{[e]}$
		3.64	3.6	0.07	86.1	37.4 ± 0.5	-163 ± 6	0.999 (0.023)
		7.29	11.7	0.14	83.6	47.4 ± 0.2	-121 ± 1	0.991 (0.098)
		14.6	58.0	0.65	80.4	57.2 ± 1.7	-78 ± 3	0.996 (0.065)
		3.64	16.4	3.35	76.7	28.5 ± 0.4	-162 ± 6	0.999 (0.010)
		7.29	32.4	4.00	77.3	64.5 ± 0.8	-43 ± 1	0.996 (0.077)
		14.6	88.0	13.9	75.2	39.8 ± 2.5	-44 ± 1	0.999 (0.015)

[a] Conversion C at 60°C on a 2 cm fused-silica column. [b] Reaction rate constant at 60°C. [c] Gibbs activation energy at 25°C. [d] Correlation factor and residual standard deviation (s.d.) of the linear regression of the Eyring plot. [e] Conversion is 100% for most data points under these conditions.

$$H = A + \frac{B}{u} + Cu \quad (3)$$

in which H is the height equivalent to a theoretical plate, u , the mean velocity of the mobile phase, A , the eddy diffusion, B , the coefficient of longitudinal diffusion, and C , the coefficient for the mass transfer. Interestingly, van Deemter originally studied the heat and mass transport in fixed catalyst beds and later transferred these derivations to chromatography, which are well-known to optimize and characterize the efficiency of a chromatographic system. Therefore, the effective plate height $H = l/N$, obtained from the capillary length l (24 m) divided by the effective plate number N , was plotted as a function of the velocity u of the carrier gas at 60 °C for the four substrates (see Figure 6). The effective plate numbers, $N = 5.545 \left(\frac{t_R - t_0}{w_h} \right)$,

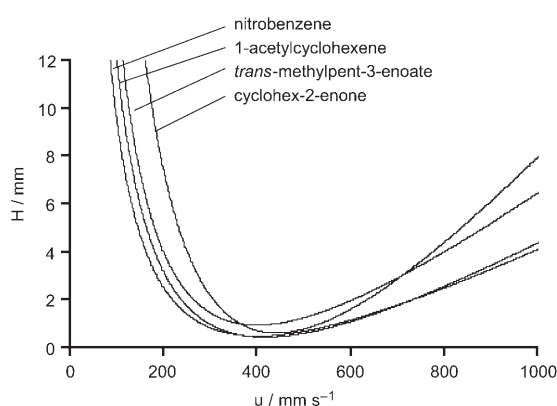


Figure 6. Determination of diffusion coefficients from van Deemter plots of the four substrates at 60 °C (precisely 2400 cm fused-silica column (injector outlet to detector inlet, i.d. 250 μ m)).

were calculated from the retention times t_R , peak width at half height, w_h , of the individual substrates, and the hold-up time, t_0 , determined from methane injections.

These curves were fitted with the van Deemter equation to obtain the constants B and C for the individual substrates. For coated capillaries, the eddy diffusion (A term) can be neglected because no additional migration paths caused by different particle sizes, shapes, and porosity such as in in packed columns have to be considered [Eq. (3)]. The B term, representing the longitudinal diffusion, directly yields the diffusion coefficients for the substrates in the mobile phase at the given temperature [Eq. (4)].

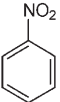
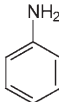
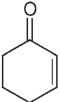
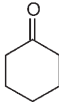
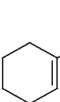
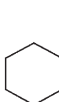
$$H = \frac{B}{u} + (C_M + C_S)u \quad \text{with} \quad B = 2D_M \quad (4)$$

$$C_M = \frac{1 + 6k' + 11k'^2}{96(1 + k')^2} \times \frac{d_c^2}{D_M}, \quad C_S = \frac{2k'}{3(1 + k')^2} \times \frac{d_f^2}{D_S}$$

The coefficient C for the mass transfer consists of the mass transfer coefficient in the mobile (C_M) and stationary phases

(C_S). D_M and D_S are coefficients of molecular diffusion in the mobile and stationary phases, respectively, d_c , the inner diameter of the capillary, and d_f , the film thickness of the stationary phase. The retention factor $k' = (t_R - t_M)/t_M$ is calculated from the retention time t_R of the substrate and the hold-up time t_M , determined by co-injection of methane. From the coefficients of the van Deemter plots, the diffusion coefficients of the substrates in the mobile phase (D_M) and in the stationary phase (D_S) were calculated. These diffusion coefficients are summarized in Table 4.

Table 4. Diffusion coefficients of the substrates in the mobile phase (D_M) and in the stationary phase (D_S) at 60 °C.

Substrate	Product	D_M [$\text{cm}^2 \text{s}^{-1}$]	D_S [$10^{-10} \text{cm}^2 \text{s}^{-1}$]
		0.14	1.82
		1.91	2.79
		0.20	0.55
		0.81	31.1

Considering these diffusion coefficients and the small paths for the substrates to migrate into the catalytically active stationary phase (film thickness 250 nm), it can be concluded that the reactions are not limited by diffusion. This means that the reaction rate constants determined in this on-column reaction chromatographic setup are directly accessible and depend only on the probability of the substrates to adsorb on Pd nanoparticles, which correlates with the concentration of the active sites in the reaction volume.

Conclusion

We have investigated hydrogenation reactions over highly active Pd nanoparticles by a synchronous combination of catalysis and separation in microcapillaries for different ratios of the stabilizing polysiloxanes, different activation temperatures, and different Pd loadings. We obtained comprehensive kinetic data from on-column chromatographic experiments by high-throughput reaction rate measurements of reactant libraries. With these data, we gained further insights into the influence of reaction parameters, for example, the particle size and stabilizing matrix. This helped us to understand the parameters controlling the mechanism and the kinetics of the investigated hydrogenation reactions over Pd nanoparticles, for example, the steric hindrance of 1-acetylcyclohexene compared to cyclohex-2-enone and *trans*-meth-

ylpent-3-enoate results in a more negative activation entropy ΔS^\ddagger , which can be explained by a more restrained transition state. Furthermore, the influence of the nature of the stabilizing matrix of the Pd nanoparticles on the catalytic activity was investigated. The employed concept of on-column reaction chromatography integrating catalyzed reactions and separation efficiency can be generally applied to other catalytic processes to characterize catalysts and materials in comprehensive kinetic studies.

Experimental Section

General methods and materials: Unless otherwise indicated, all reactions were performed under an argon atmosphere by using standard Schlenk techniques. All chemicals were obtained from Fluka (Buchs, Switzerland) or Sigma-Aldrich (Steinheim, Germany) and used as received. GE SE 52 was purchased from Macherey-Nagel (Düren, Germany). All solvents were dried by using standard techniques. Fused-silica capillaries (i.d. 250 μm , o.d. 365 μm) were purchased from Microquartz (Munich, Germany).

Analytical techniques: Nuclear magnetic resonance (^1H NMR and ^{13}C NMR) spectra were recorded in CDCl_3 on a Bruker DPX 300 spectrometer (Rheinstetten, Germany) either at 300 and 75 MHz, respectively, or on a Bruker AV 400 spectrometer (Rheinstetten, Germany) at 400 and 100 MHz, respectively. On-column reaction gas chromatographic measurements were performed on a Thermo Trace PolarisQ GC-MS apparatus equipped with a split injector (250 °C) and a flame ionization detector (250 °C). Hydrogen (5.0) was used as reactive carrier gas. The measurements were repeated three times at each temperature in steps of 10 K. Transmission electron micrographs were obtained on a Hitachi 7500 microscope operating with an acceleration voltage of 100 kV. High-resolution transmission electron microscopy (HRTEM) images were obtained on a Hitachi HF 2000 microscope with a cold field-emission source operating at 200 keV.

Hydridomethylsiloxane-dimethylsiloxane copolymer: A mixture of hexamethyldisiloxane (8.1 g, 50.0 mmol), polyhydridomethylsiloxane (6.0 g, 100.0 mmol), octamethylcyclotetrasiloxane (66.7 g, 225.0 mmol), china clay (2 g), and sulfuric acid (1 mL) was stirred at 100 °C under gentle reflux for 5 d. During this time, the reaction mixture became increasingly more viscous. After cooling the mixture to room temperature, the catalyst (china clay + sulfuric acid) was removed by extraction with water and filtration. Water and other volatile constituents of the filtrate were removed by evaporation at 120 °C under an oil-pump vacuum to give HMPS (62.6 g, 78.3%). ^1H NMR (300 MHz, CDCl_3 , 25 °C): $\delta = -0.02$ – 0.25 (m; $\text{Si}(\text{CH}_3)_n$ ($n=1-3$)), 4.61 ppm (s, SiH); ^{13}C NMR (100 MHz, CDCl_3 , 25 °C): $\delta = -2.3$, 1.3, 1.6 ppm; by integration of the signals of the ^1H NMR spectrum, the total content of $\text{Si}(\text{O})(\text{CH}_3)\text{H}$ groups was determined to be 25.7%.

Methylvinylsiloxane-dimethylsiloxane copolymer: Diethoxymethylvinylsilane (4.3 g, 26.9 mmol) and diethoxydimethylsilane (35.9 g, 242.0 mmol) were mixed and sodium hydroxide (0.5 g) dissolved in a mixture of water (50 mL) and ethanol (50 mL) was added dropwise at 0 °C. The mixture was stirred for 1 h, then heated to 60 °C for 5 h. Chlorotrimethylsilane (0.9 g, 8.1 mmol) was added slowly for end-capping and the mixture was stirred for 24 h. The product was extracted with *n*-pentane and washed with water. The organic phase was separated and the solvent was removed by rotary evaporation. The product was dried under high vacuum at 60 °C to give MVPS (14.8 g, 69.2%). ^1H NMR (300 MHz, CDCl_3 , 25 °C): $\delta = -0.03$ – 0.09 (m; $\text{Si}(\text{CH}_3)_n$ ($n=1-3$)), 5.69–5.99 ppm (m; $\text{Si}-\text{CH}=\text{CH}_2$); ^{13}C NMR (100 MHz, CDCl_3 , 25 °C): $\delta = 136.1$, 132.0, 131.7, 56.7, 17.3, 0.0 ppm; by integration of the signals of the ^1H NMR spectrum, the total content of $\text{Si}(\text{O})(\text{CH}_3)(\text{CH}=\text{CH}_2)$ groups was determined to be 4.5%.

Preparation of Pd nanoparticles in a polysiloxane matrix and coating of microcapillaries: Palladium acetate, HMPS, MVPS, and GE SE 52 (Macherey-Nagel, containing 5% phenyl groups) were mixed in absolute diethyl ether in the ratios given in Tables 1 and 2. Fused-silica capillaries (length 5 m, thermally deactivated at 220 °C for 24 h) were coated with these solutions. The reaction course was followed by ^1H NMR spectroscopy for the SiH group. ^1H NMR (300 MHz, CDCl_3 , 25 °C): $\delta = -0.20$ – 0.19 (m; $\text{Si}(\text{CH}_3)_n$ ($n=1-3$)), 4.61 ppm (s, SiH); by integration of the signals of the ^1H NMR spectrum, the total content of $\text{Si}(\text{O})(\text{CH}_3)\text{H}$ groups was determined.

Capillaries were coated by the static method described by Grob^[23] to obtain a uniform film with a thickness of 250 nm. Therefore, fused-silica capillaries (i.d. 250 μm) were filled with the respective polymer solution in diethyl ether and the solvent was removed by high vacuum after closing one end of the capillary. Then the capillaries were flushed with argon and the polymer film was immobilized in a slow hydrogen stream while heating the capillary from 25 to 200 °C at a rate of 0.5 K min^{-1} . The temperature was maintained for 8 h.

On-column hydrogenation: On-column hydrogenation experiments were performed on a Thermo Trace PolarisQ GC-MS apparatus equipped with a split injector (250 °C), a flame ionization detector (250 °C), and a quadrupole ion-trap mass spectrometer. For the hydrogenation of different substrates, fused-silica capillaries coated with Pd nanoparticles embedded in a polysiloxane matrix (2.02–6.15 $\text{cm} \times 250 \mu\text{m}$ i.d., 0.25 μm film thickness) were employed. These capillaries were coupled between a pre-separation column (HP-5, 1 $\text{m} \times 250 \mu\text{m}$ i.d.) and a separation column (HP-5, 25 $\text{m} \times 250 \mu\text{m}$ i.d.) to quantify the reaction mixture. Hydrogen was used as a carrier gas. All measurements were repeated three times at each temperature (60, 70, 80, 90, and 100 °C) and pressure (60, 70, 80, 90, and 100 kPa). A total of 375 measurements were considered for the statistical analysis of the reaction rate constants to obtain activation parameters.

Acknowledgements

Generous financial support by an Emmy Noether grant of the Deutsche Forschungsgemeinschaft (DFG TR 542/3), the Max-Planck-Institut für Kohlenforschung, the Fonds der Chemischen Industrie (FCI), and the Merck Research Laboratories (Rahway, New Jersey, USA) is gratefully acknowledged. S.K.W. thanks the Cusanuswerk for a doctorate scholarship. We thank Dr. B. Tesche and A. Dreier for TEM, SEM, and EDX measurements.

- [1] P. L. Hansen, J. B. Wagner, S. Helveg, J. R. Rostrup-Nielsen, B. S. Clausen, H. Topsøe, *Science* **2002**, 295, 2053.
- [2] C. T. Campbell, *Nature* **2004**, 432, 282.
- [3] a) L. Razon, R. Schmitz, *Chem. Eng. Sci.* **1986**, 41, 1561; b) F. C. Moates, M. Somani, J. Annamalai, J. T. Richardson, D. Luss, R. C. Willson, *Ind. Eng. Chem. Res.* **1996**, 35, 4801; c) A. Holzwarth, H.-W. Schmidt, W. F. Maier, *Angew. Chem.* **1998**, 110, 2788; *Angew. Chem. Int. Ed.* **1998**, 37, 2644; d) M. T. Reetz, M. H. Becker, K. M. Kühling, A. Holzwarth, *Angew. Chem.* **1998**, 110, 2792; *Angew. Chem. Int. Ed.* **1998**, 37, 2647; e) S. J. Taylor, P. J. Morken, *Science* **1998**, 280, 267; f) S. S. Lasko, R. J. Hendershot, J. Reed, Y. Fu, M.-F. Fellmann, G. Oskarsdottir, C. M. Snively, J. Lauterbach in *High-Throughput Analysis: Spectroscopic Imaging in the Mid-Infrared Applied to High-Throughput Studies of Supported Catalyst Libraries* (Eds.: R. A. Potyrailo, E. Amis), Kluwer Academic, New York, **2003**, p. 77; g) J. Klein, W. Stichert, W. Strehlau, A. Brenner, D. Demuth, S. A. Schunk, H. Hibst, S. Storck, *Catal. Today* **2003**, 81, 329; h) S. Cypes, A. Hagemeyer, Z. Hogan, A. Lesik, *Comb. Chem. High Throughput Screening* **2007**, 10, 25.
- [4] S. M. Senkan, S. Ozturk, *Angew. Chem.* **1999**, 111, 867; *Angew. Chem. Int. Ed.* **1999**, 38, 791.

- [5] a) P. Cong, R. D. Doolen, Q. Fan, D. M. Giaquinta, S. Guan, E. W. McFarland, D. M. Poojary, K. Self, H. W. Turner, W. H. Weinberg, *Angew. Chem.* **1999**, *111*, 507; *Angew. Chem. Int. Ed.* **1999**, *38*, 483; b) M. Orschel, J. Klein, H.-W. Schmidt, W. F. Maier, *Angew. Chem.* **1999**, *111*, 2961; *Angew. Chem. Int. Ed.* **1999**, *38*, 2791; c) S. Senkan, K. Krantz, S. Ozturk, V. Zengin, I. Onal, *Angew. Chem.* **1999**, *111*, 2965; *Angew. Chem. Int. Ed.* **1999**, *38*, 2794; d) M.-J. Kang, A. Tholey, E. Heinzle, *Rapid Commun. Mass Spectrom.* **2001**, *15*, 1327; e) H. Wang, Z. Liu, J. Shen, *J. Comb. Chem.* **2003**, *5*, 802.
- [6] a) A. C. Cooper, L. H. McAlexander, D.-H. Lee, M. T. Torres, R. H. Crabtree, *J. Am. Chem. Soc.* **1998**, *120*, 9971; b) E. Reddington, A. Sapienza, B. Gurau, R. Viswanathan, S. Sarangapani, E. S. Smotkin, T. E. Mallouk, *Science* **1998**, *280*, 1735.
- [7] a) M. T. Reetz, A. Zonta, K. Schimossek, K. Liebeton, K.-E. Jaeger, *Angew. Chem.* **1997**, *109*, 2961; *Angew. Chem. Int. Ed. Engl.* **1997**, *36*, 2830; b) M. T. Reetz, K.-E. Jaeger, *Top. Curr. Chem.* **1999**, *200*, 31; c) M. T. Reetz, K.-E. Jaeger, *Chem. Eur. J.* **2000**, *6*, 407; d) P. G. Schultz, R. A. Lerner, *Science* **1995**, *269*, 1835; e) F. Zoicher, M. M. Enzelberger, U. T. Bornscheuer, B. Hauer, R. D. Schmid, *Anal. Chim. Acta* **1999**, *391*, 345; f) E. Henke, U. T. Bornscheuer, *Biol. Chem.* **1999**, *380*, 1029.
- [8] a) A. P. de Silva, H. Q. N. Gunaratne, T. Gunnlaugsson, A. J. M. Huxley, C. P. McCoy, J. T. Rademacher, T. E. Rice, *Chem. Rev.* **1997**, *97*, 1515; b) G. Zandonella, L. Haalck, F. Spener, K. Faber, F. Paltauf, A. Hermetter, *Chirality* **1996**, *8*, 481; c) G. Gauglitz, *Curr. Opin. Chem. Biol.* **2000**, *4*, 351; d) M. Olsen, B. Iverson, G. Georgiou, *Curr. Opin. Biotechnol.* **2000**, *11*, 331; e) R. P. Hertzberg, A. J. Pope, *Curr. Opin. Chem. Biol.* **2000**, *4*, 445.
- [9] C. Hoffmann, A. Wolf, F. Schüth, *Angew. Chem.* **1999**, *111*, 2971; *Angew. Chem. Int. Ed.* **1999**, *38*, 2800.
- [10] R. A. Potyrailo, R. J. May, *Rev. Sci. Instrum.* **2002**, *73*, 1277.
- [11] O. Trapp, *J. Chromatogr. A* **2008**, *1184*, 160–190.
- [12] S. J. Haswell, P. Watts, *Green Chem.* **2003**, *5*, 240.
- [13] a) C. de Bellefon, N. Tanchoux, S. Caravieilhès, P. Grenouillet, V. Hessel, *Angew. Chem.* **2000**, *112*, 3584; *Angew. Chem. Int. Ed.* **2000**, *39*, 3442; b) J. Knight, *Nature* **2002**, *418*, 474; c) A. Müller, K. Drese, H. Gnaser, M. Hampe, V. Hessel, H. Löwe, S. Schmitt, R. Zapf, *Catal. Today* **2003**, *81*, 377; d) K. Jähnisch, V. Hessel, H. Löwe, M. Baerns, *Angew. Chem.* **2004**, *116*, 410; *Angew. Chem. Int. Ed.* **2004**, *43*, 406; e) D. Belder, M. Ludwig, L.-W. Wang, M. T. Reetz, *Angew. Chem.* **2006**, *118*, 2523; *Angew. Chem. Int. Ed.* **2006**, *45*, 2463; f) D. Janasek, J. Franzke, A. Manz, *Nature* **2006**, *442*, 374; g) S. J. Haswell, *Nature* **2006**, *441*, 705.
- [14] O. Trapp, S. K. Weber, S. Bauch, W. Hofstadt, *Angew. Chem.* **2007**, *119*, 7447; *Angew. Chem. Int. Ed.* **2007**, *46*, 7307.
- [15] M. R. Arnold, *Chem. Eng. Rev.* **1956**, *48*, 1629.
- [16] a) H. Bönemann, W. Brijoux, R. Brinkmann, E. Dinjus, T. Joujen, B. Korall, *Angew. Chem.* **1991**, *103*, 1344; *Angew. Chem. Int. Ed. Engl.* **1991**, *30*, 1312; b) M. T. Reetz, W. Helbig, S. A. Quaiser, U. Stimming, N. Breuer, R. Vogel, *Science* **1995**, *267*, 367; c) H. Bönemann, G. A. Braun, *Angew. Chem.* **1996**, *108*, 2120; *Angew. Chem. Int. Ed. Engl.* **1996**, *35*, 1992; d) H. Bönemann, R. M. Richards, *Eur. J. Inorg. Chem.* **2001**, 2455.
- [17] a) J. Kobayashi, Y. Mori, K. Okamoto, R. Akiyama, M. Ueno, T. Kitamori, S. Kobayashi, *Science* **2004**, *304*, 1305; b) D. Astruc, F. Lu, J. R. Aranzas, *Angew. Chem.* **2005**, *117*, 8062; *Angew. Chem. Int. Ed.* **2005**, *44*, 7852.
- [18] a) M. T. Reetz, E. Westermann, *Angew. Chem.* **2000**, *112*, 170; *Angew. Chem. Int. Ed.* **2000**, *39*, 165; b) M. T. Reetz, J. G. D. Vries, *Chem. Commun.* **2004**, 1559; c) D. Astruc, *Inorg. Chem.* **2007**, *46*, 1884; d) K. Köhler, W. Kleist, S. S. Pröckl, *Inorg. Chem.* **2007**, *46*, 1876.
- [19] D. Teschner, E. Vass, M. Hävecker, S. Zafeirotas, P. Schnörch, H. Sauer, A. Knop-Gericke, R. Schlögl, M. Chamam, A. Wootsch, A. S. Canning, J. J. Gamman, S. D. Jackson, J. McGregor, L. F. Gladden, *J. Catal.* **2006**, *242*, 26.
- [20] B. P. S. Chauhan, J. S. Rathore, T. Bando, *J. Am. Chem. Soc.* **2004**, *126*, 849.
- [21] H. Figge, A. Deege, J. Köhler, G. Schomburg, *J. Chromatogr.* **1986**, *351*, 393.
- [22] W. Lu, B. Wang, K. Wang, X. Wang, J. G. Hou, *Langmuir* **2003**, *19*, 5887.
- [23] K. Grob, *Making and Manipulating Capillary Columns for Gas Chromatography*, Huethig, Heidelberg (Germany), **1986**.
- [24] a) T. Falk, A. S. -Morgenstern, *Chem. Eng. Sci.* **1999**, *54*, 1479; b) T. D. Vu, A. Seidel-Morgenstern, S. Grüner, A. Kienle, *Ind. Eng. Chem. Res.* **2005**, *44*, 9565.
- [25] A. Seidel-Morgenstern, *J. Chromatogr. A* **2004**, *1037*, 255.
- [26] a) T. Haas, J. Gaube, *Chem. Eng. Technol.* **1989**, *12*, 45; b) M. Di Serio, V. Balato, A. Dimiccoli, L. Maffucci, P. Iengo, E. Santacesaria, *Catal. Today* **2001**, *66*, 403; c) A. Schmidt, R. Schomäcker, *Ind. Eng. Chem. Res.* **2007**, *46*, 1677.
- [27] a) H. Wieland, *Chem. Ber.* **1912**, *45*, 484; b) N. Zelinsky, N. Pavlov, *Chem. Ber.* **1923**, *56B*, 1249; c) R. P. Linstead, S. L. S. Thomas, *J. Chem. Soc.* **1940**, 1127.
- [28] a) J. J. van Deemter, *Ind. Eng. Chem.* **1953**, *45*, 1227; b) J. J. van Deemter, *Ind. Eng. Chem.* **1954**, *46*, 2300; c) J. J. van Deemter, F. J. Zuiderweg, A. Klinkenberg, *Chem. Eng. Sci.* **1956**, *5*, 271; d) J. J. van Deemter, *Chem. Eng. Sci.* **1961**, *13*, 143; e) S. J. Hawkes, *J. Chem. Educ.* **1983**, *60*, 393.

Received: November 12, 2007
Published online: April 2, 2008